

DYNAMIC CHARACTERISTICS OF FLOATING OFFSHORE STRUCTURE SPAR-TYPE WIND TURBINES UNDER REGULAR AND IRREGULAR WAVES

Ashraf Mohammed Abou-Rayan¹, Hala Mohammed Refaat², Behairy Ahmed Behairy³ & Ahmed Youssef Kamal⁴

^{1,2}Professor, Department of Civil Engineering, Benha University, Egypt

⁴Assistant Professor, Department of Civil Engineering, Benha University, Egypt

³Graduate Student, Department of Civil Engineering, Benha University, Egypt

ABSTRACT

Egypt is one of the best places in the world to find wind power. With wind speeds at average 8.5 to 10 m/sec, Egypt is at the forefront in the region in terms of wind power. In this investigation a Spar-Type offshore structure equipped with 5MW wind turbine have been considered. The dynamic motion responses are critical for designing the substructures of Spar-Type wind turbines. All environmental loads from waves and wind have been considered in this investigation. The available data for the Gulf of Suez area from the Egyptian Meteorological Authority was used to determine the environmental loads. For the dynamic study, the analysis software ANSYS-AQWA was used to determine out the hydrodynamic properties, FAST simulation software for wind turbine, and MATLAB software for the spectral analysis. The results of the investigation help to better understand the stability and dynamic response of Spar-Type wind turbines. Time history, Power Spectrum Density, and phase plan are included in the results.

KEYWORDS: *Off Shore Wind Turbines, Spar-Type Offshore Structure, Wave Forces, Wind Forces, Coupled Analysis, Dynamic Response*

Article History

Received: 11 Jul 2023 | Revised: 23 Aug 2023 | Accepted: 30 Aug 2023

Abbreviations

FOWT	Floating offshore wind turbines
TLP	Tension leg platform
BEM	Blade element momentum
FEM	Finite Element Method
SFWT	Spar floating wind turbine
RAO	Response Amplitude Operator
FFT	Fast Fourier Transform
LC	Load Case
EMA	Egyptian Meteorological Authority

WHA Wave Heading Angle

SD Standard Deviation

1. INTRODUCTION

Recently, the demand for renewable power is growing quickly around the world because of climate change and the limited supply of oil. Wind energy appears to be a clean and viable option for meeting a large portion of this energy need. Most of the world is potentially able to get renewable energy from floating offshore wind turbines (FOWT) due to the huge wind resource in deep-water. Egypt has a lot of places where can get wind energy, certainly the Gulf of Suez. Offshore wind turbines experience higher and more steady wind speeds than wind turbines on land. Fixed and floating offshore wind farms are used to both shallow and deep-water regions. The floating types include tension leg platforms (TLP), spar platforms, semi-submersible platforms, etc., while the fixed types include gravity supports, monopile supports, tripod supports, etc. In Europe, there are several offshore wind projects that are built on fixed bases (Shin, 2011). Some of the most efficient solutions to build offshore wind farms in the future are movable wind turbines with hulls that are similar to those used in the offshore oil and gas industry (Duan et al., 2016). Díaz and Guedes Soares (2020) showed an increase in the size of wind farms and the capacity of turbines for making electricity from wind, which makes the offshore wind industry more promising and appealing for the future. Since the European Union plans up to 100 GW of offshore wind electricity by 2030, the entire installed capacity will continue rising up (Soares-Ramos et al., 2020). Bashir (2022) examined the fundamental variables that govern wind turbine performance, such as energy use, material use, recycling strategies, and environmental effects. As a result, in order to determine out how safe and reliable FOWTs are in deep oceans, it is important to study the system of FOWT and wind-wave actions as an entire system. Extensive studies on the dynamical responses and characteristics of the FOWTs has been carried out in recent decades.

Matsukuma and Utsunomiya (2008) analysed the motion of a floating Spar-Type carrying a 2 MW turbine under winds. They used multibody dynamics system theory. Jonkman and Matha (2011) examined three FOWT designs utilising FAST simulation tool with AeroDyn and HydroDyn. Myhr et al. (2011) performed wave tank experiments using Tension-Leg-Buoy floater compared to the OC3-Hywind Spar at the NTNU/MARINTEK MCLab that was also extended with simulations using the models 3Dfloat and ANSYS. Karimirad and Moan (2012) analysed motions of a 5-MW Spar-Type FOWT in environmental conditions for combined wave and wind-induced. They found that the standard deviations of the dynamic responses are mostly caused by waves, whereas the mean values of the responses are caused mainly by wind. Jeon et al. (2013) investigated numerical analysis of the dynamic response of a Spar-Type to irregular wave while assuming the irregular wave is generated according to the Pierson-Moskowitz spectrum. By combining blade element momentum (BEM) and finite element method (FEM) in a staggered iterative manner, they were able to simulate the interactions between waves and floating substructures and waves and mooring cables. Sethuraman and Venugopal (2013) used time-domain modelling tool OrcaFlex to evaluate their experimental measurements of the responses of a spar floating wind turbine (SFWT) under regular and irregular waves. They measured their observed hydrodynamic responses to numerical simulations using the Response Amplitude Operator (RAO). Hussein et al. (2013) performed A 3D finite element analysis of the floating foundation of the WindFloat concept using ANSYS software including the weight of the tower, the wind thrust force, and all environmental loads in the Red Sea. Abou-Rayan and El-Gamal (2013) conducted a numerical analysis in the time domain to examine the impact of hydrodynamic force-related nonlinearities and the influence of all degrees of freedom being coupled together on a TLP's dynamic response. Abou-Rayan and Hussein (2014)

studied the Square TLP nonlinear response to random waves produced using the Pierson-Moskowitz spectrum. They concluded that when uni-directional waves in the surge direction were taken into account surge, heave, and pitch degrees-of-freedom responses are affected. Oyejobi et al. (2017) compared the dynamic response of a TLP with intact tendons to one with the tendons removed while subjected to random wave and current loads in two different sea conditions. Yu et al. (2015) used the numerical simulation code FAST in the time domain to study the hydrodynamic properties of the OC3-Hywind concept, as well as the dynamic response. The frequency analysis was performed using the fast fourier transform (FFT) method. Abou-Rayan et al. (2016) used ANSYS-AQWA, FAST, and MATLAB software to compare the dynamic response of triangular, square, and pentagonal TLP geometries under multi-directional regular and random waves. Yue et al. (2020) developed the coupled aerodynamic - hydrodynamic - mooring line system model using FORTRAN language and hydrodynamic software AQWA. Zheng et al. (2020) carried out a hydrodynamic analysis on a moored 6MW Spar-Type FOWT, taking into account the interaction between the wave, current, and the structure in regular waves and uniform current. Qu et al. (2020) developed an in-house MATLAB code considering the effect of aerodynamics, hydrodynamics, and mooring to make numerical investigations. Tafazzoli et al. (2021) investigated a mooring system for the SFWT consisting of chain-cable-chain. For heave, roll, pitch, and yaw responses five chain lengths from 25 to 65 m were investigated. Wen et al. (2022) developed a model Spar-Type FOWT and an experiment to demonstrate the aerodynamic loading effects. The increased aerodynamic loading seems to suppress the pitch resonance vibration while amplifying the resonance vibration at surge frequency.

This study compares the performance of a new model spar (Model I) to the (OC3-Hywind) spar developed by, Jonkman (2010) under combined wind and wave actions. Both spars are equipped with a 5-MW NREL standard wind turbine refer to, Jonkman et al. (2009). The paper is structured up as the following. First, the explanation of the numerical model for the FOWT. Environmental conditions of wind and wave are the n explained. Then using ANSYS-AQWA and FAST to simulate the dynamic responses of the FOWT Finally, some brief conclusions are suggested.

2. DESCRIPTIONS OF THE SPAR-TYPE OFFSHORE STRUCTURE

The wind turbine floats through a steel cylinder filled with ballast that keeps the centre of gravity far below the centre of buoyancy. This creates a large righting moment arm and a large amount of inertial resistance to pitch and roll movements. Permanent solid iron ballast, concrete, or gravel are used to ballast the floater. An anchor chain, steel cable, and/or synthetic fiber rope catenary spread mooring system is typically used to anchor the SFWT. Tables 1 and 2 show the properties of the wind turbine and the Spar-Type support platform, which are used to determine the properties of the whole SFWT system. Table 3, provides information about the mooring lines' specific characteristics. The platform's pitch angle, which must be less than 5 degrees, and the natural periods of heave and pitch, which must be longer than 20–30 seconds according to Crozier (2011), use it as constraints that help define the design space of the platform specification. Figure: 1 illustrates the detailed information of (Model-I) Spar-Type wind turbine.

Table 1: Parameters of NREL 5-MW Baseline Wind Turbine. Jonkman et al. (2009)

Item	Properties
Rating	5 MW
Rotor Orientation, Configuration	Upwind, 3 Blades
Rotor, Hub Diameter	126 m, 3 m
Hub Height	90 m
Cut-In, Rated, Cut-Out Wind Speed	3 m/s, 11.4 m/s, 25 m/s
Rated Tip Speed	80 m/s
Rotor Mass	110,000 kg
Nacelle Mass	240,000 kg
Tower Mass	347,460 kg
Coordinate Location of Overall CM	(-0.2 m, 0.0 m, 64.0 m)

Table 2: Parameters of Spar-Type Floating Platform

Item	OC3-Hywind	Model I
Depth to Platform Base Below SWL (Total Draft)	120 m	80 m
Elevation to Platform Top (Tower Base) Above SWL	10 m	10 m
Depth to Top of Taper Below SWL	4 m	4 m
Depth to Bottom of Taper Below SWL	12 m	12 m
Platform Diameter Above Taper	6.5 m	6.5 m
Platform Diameter Below Taper	9.4 m	13.09 m
Platform Mass, Including Ballast	7,466,330 kg	9,435,000 kg
CM Location Below SWL Along Platform Centerline	89.91 m	66.8 m

Table 3: Parameters of Catenary Mooring Lines

Item	OC3-Hywind	Model I
Number of Mooring Lines	3	3
Angle Between Adjacent Lines	120 °	120 °
Depth to Anchors Below SWL (Water Depth)	320 m	320 m
Depth to Fairleads Below SWL	70 m	45 m
Radius to Anchors from Platform Centerline	853.87 m	853.87 m
Radius to Fairleads from Platform Centerline	5.2	6.545 m
Unstretched Mooring Line Length	902.2	909.4 m
Mooring Line Diameter	0.09 m	0.09 m
Equivalent Mooring Line Mass Density	77.7066 kg/m	77.7066 kg/m
Equivalent Mooring Line Weight in Water	698.094 N/m	698.094 N/m
Equivalent Mooring Line Extensional Stiffness	384,243,000 N	384,243,000 N

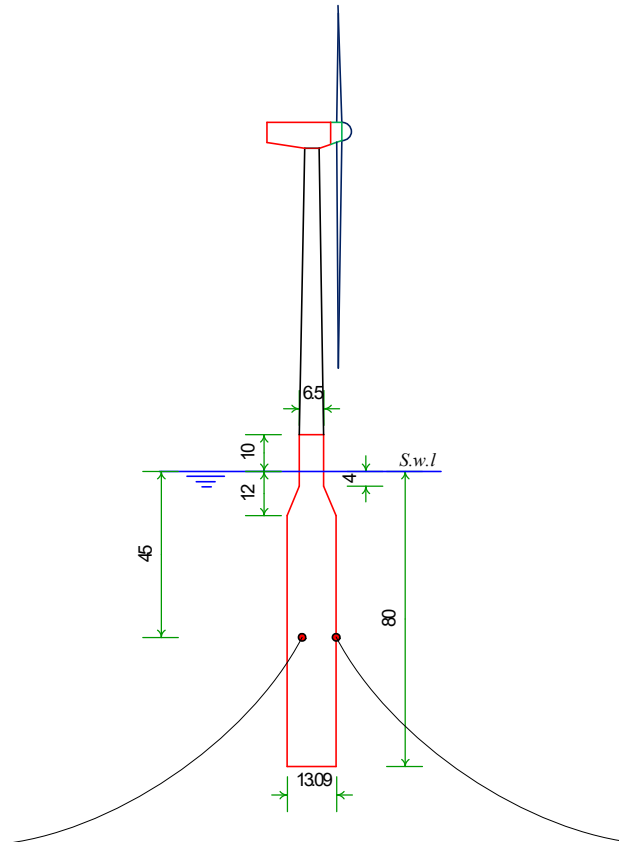


Figure 1: Model I Spar-Type Wind Turbine.

3. NUMERICAL MODEL

For the dynamic response, we used the commercial FEM software ANSYS-AQWA, which is part of the ANSYS software package. The hydrostatic loads were determined through the AQWA hydrodynamic diffraction model. The results of AQWA hydrodynamic diffraction been inserted into ANSYS AQWA hydrodynamic time response with other external loads like wind, wave, and mooring line load [Ansys \(2016\)](#). The blade element momentum (BEM) theory could be used to determine the aerodynamic loads on the rotor of a wind turbine. This theory divides the blade into parts and applies the formula of momentum to calculate out the aerodynamic loads on each part [Jonkman and Buhl Jr \(2005\)](#). The force from the FAST modelling at the base of the tower are then sent to the ANSYS-AQWA software to simulate the SFWT response.. In this study, both regular and irregular waves are considered. The wave spectrum from the Joint North Sea Wave Project (JONSWAP) is used to represent irregular waves [Hasselmann et al. \(1973\)](#). A Summary of coupled dynamic analysis for the SFWT is shown in Figure: 2 The hydrodynamic model of the two models of SFWT built in ANSYS-AQWA are shown in Figure: 3. Table: 4 shows that the natural frequencies in this study are very similar to those in the OC3-Hywind analysis, which proves that the SFWT model made in ANSYS-AQWA is reliable.

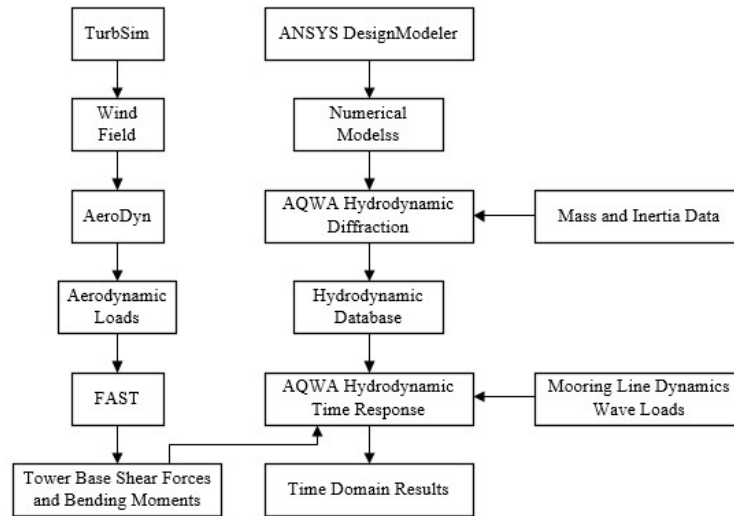
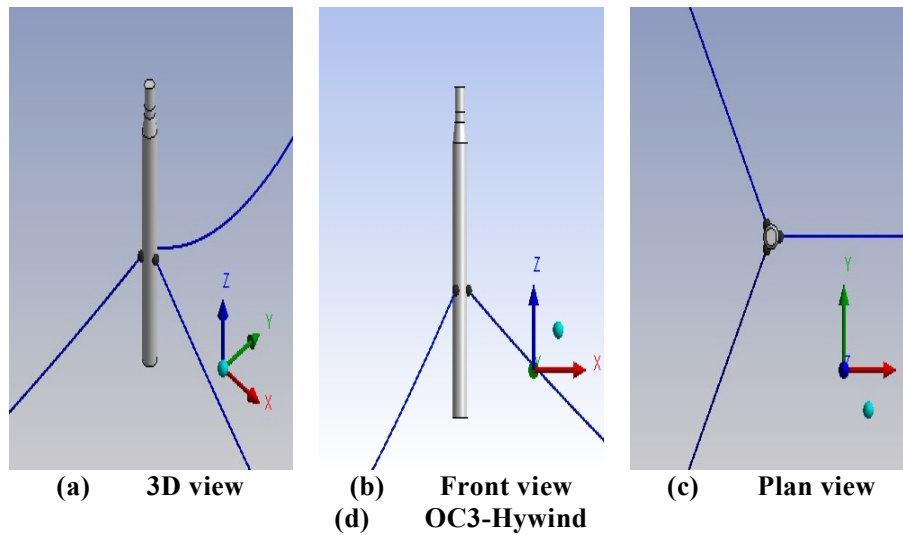


Figure 2: Flowchart of Time-Domain Coupled Analysis.

Table 4: Comparison of Natural Frequency

Motion Mode	Natural Frequency in OC3-Hywind Project (HZ)	Natural Frequency in OC3-Hywind using AQWA (HZ)	Natural Frequency in Model I using AQWA (HZ)
Surge	0.0080	0.0083	0.0072
Heave	0.0324	0.0455	0.0411
Pitch	0.0343	0.0327	0.0389



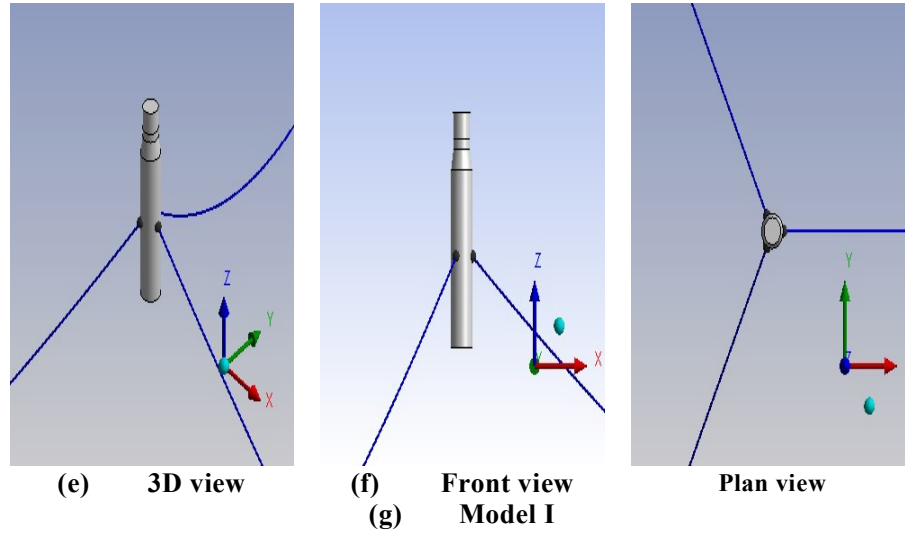


Figure 3: Hydrodynamic Models in ANSYS-AQWA.

4. ENVIRONMENTAL CONDITIONS

The available data from the Egyptian Meteorological Authority (EMA) was used to determine the environmental conditions. Where the EMA stated the highest conditions were, maximum wave height of 4m and maximum wind speed of 9.0m/sec. In this study, the wave height, wave period, and steady wind speed were all set to 5m, 10s, and 10.0m/sec, respectively. Note that the speed of the wind was measured in the direction of the wave. Wave heading angles (WHA) of 0°, 30°, 60°, and 90° were used to represent a regular wave's forces operating on many directions. See Figure: 4

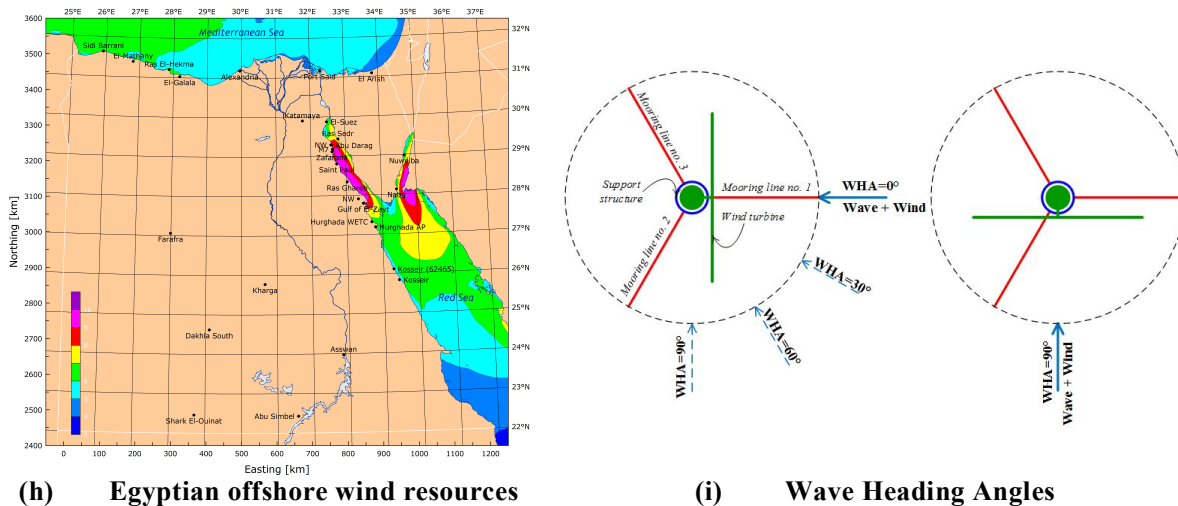


Figure 4: Environmental Data.

5. LOAD CASES

The dynamic motions of these two models under various conditions are calculated so that the results can be studied. Table 5 shows the main load case characteristics, where H is the height of the waves and T is the time for waves. Linear Airy wave theory is used to produce regular waves, and the JONSWAP spectrum describes irregular waves. V is the velocity for uniform wind.

Table 5: Comparison of Natural Frequency

Load Case	Wave Condition	H (m)	T (s)	WHA (degree)	Wind Condition	V (m/s)
LC 1	Regular wave	5	10	0,30,60,90	-	-
LC 2	Regular wave	5	10	0,90	uniform	10 m/s
LC 3	Irregular wave	5	10	0	-	-

6. RESULTS AND DISCUSSIONS

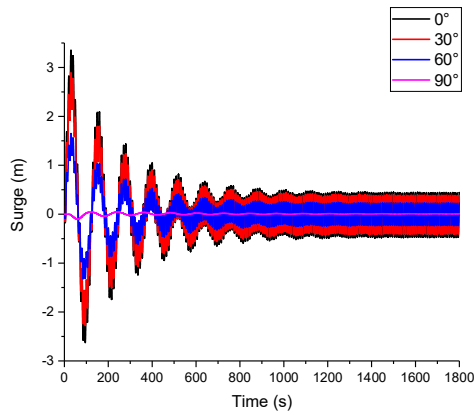
In this section, a series of comparison of dynamic responses between these two models are carried out in wave-only case and combined wind-wave cases, respectively. Throughout this work, understanding the dynamic characteristics and differences of these two models can improve the stability and performance of SFWT's, and contributes to the design of a new model of floating wind turbines. There are six degrees of freedom (DOFs) in the rigid body platform. These are surge, sway, heave, roll, pitch, and yaw. Overall, the platform's responses to surge, heave, and pitch are very obvious of the whole system. There is enormous response data, but only the effective response will be shown. The other response data may not be relevant. The surge, heave, and pitch motions of the platform are being examined.

6.1 REGULAR WAVE

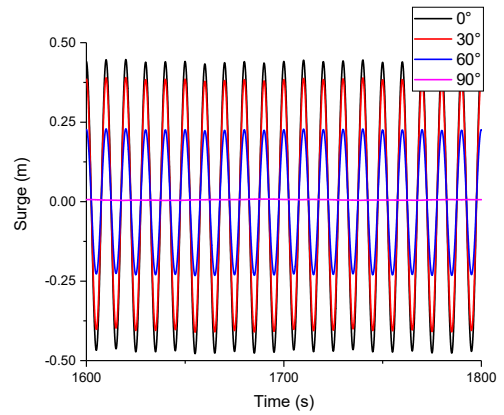
As mentioned in table 5, two cases will be examined under regular wave; load case 1 (LC 1), where the structure will be analyzed under wave only and load case 2 (LC 2), where the structure will be analyzed under wave and wind.

6.1.1 Surge Response (LC 1)

Displacement time histories, Power spectrum densities and phase planes for the two models of SFWT's are presented in figures 5, 6 and 7, at 10 sec. wave period and 5m wave height. Figure: 5, shows that the surge transient response for the floating body takes about 500 sec. to reach stationary state response, which means that the transient response is critical. The surge motion of the OC3-Hywind model is shown in Figure: 5 under different WHA (30, 60, and 90 degrees), It is obvious that waves of zero heading angles give the maximum response. The response decreases when the WHA increase (30, 60, and 90 degrees) as shown in Figure: 5-b. The surge motion of the OC3-Hywind model is smaller than that in the Model I as shown in Figure: 5-a, indicating that when the spar draft (Height of the spar Platform Below SWL) increases the surge motion decrease, where the height of the OC3-Hywind model (120 m) is larger than the Model I (80 m) by 33.3% and the Model I mass is larger than the OC3-Hywind model by 26.3% as shown in table 2. It is clear from the Power spectrum densities for the two models of SFWT's in Figure: 6-b that the response has a periodic pattern with maximum peak response at the wave excitation frequency (about 0.1 HZ) The phase planes of the two models of SFWT's shown in Figure: 7 shows that the steady state behavior is periodic and stable.

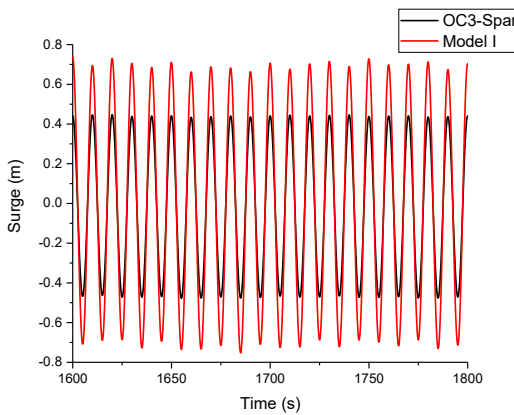


(j) Surge Motion from 0 to 1800 s

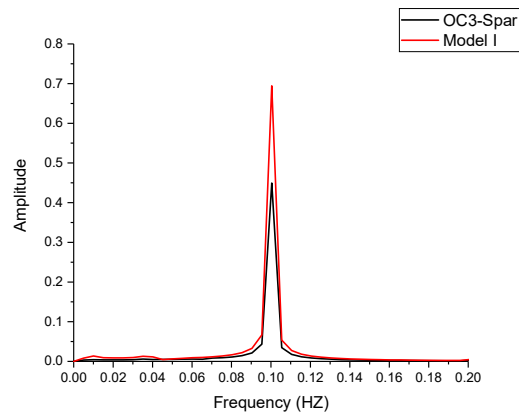


(k) Surge Motion from 1600 s to 1800 s

Figure 5: Surge response under LC 1, WHA= 0°, 30°, 60° and 90° for OC3-Hywind.

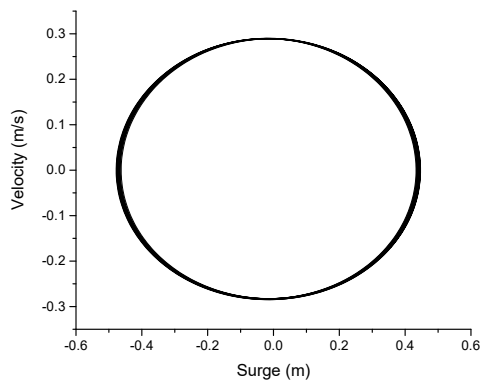


(l) Surge Motion from 1600 s to 1800 s.

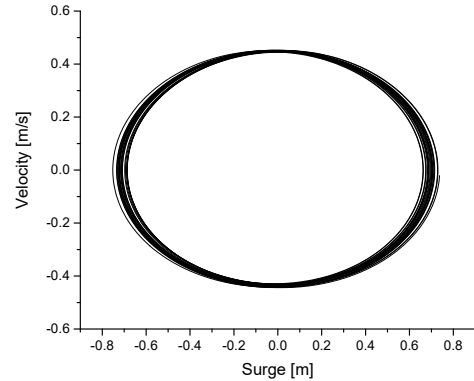


(m) Power Spectrum Density.

Figure 6: Surge Response under LC 1, WHA= 0°, 30°, 60° and 90° for OC3-Hywind.



(n) Phase Plan for OC3-Hywind

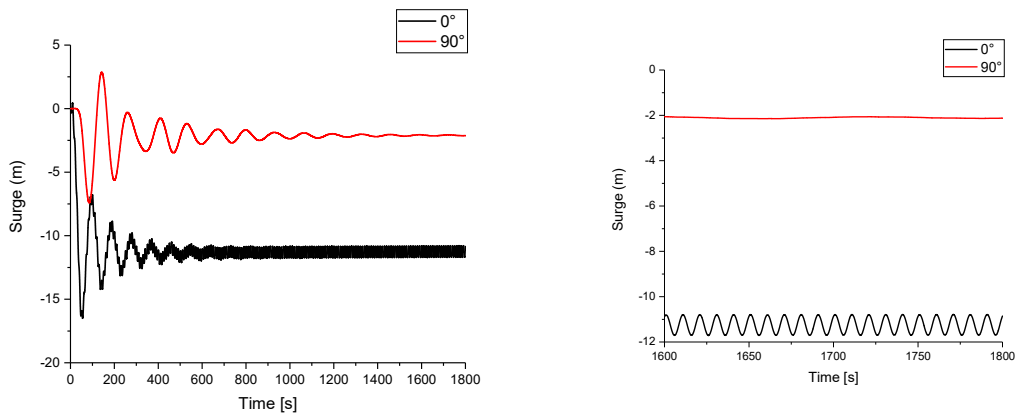


(o) Phase Plan for Model-I

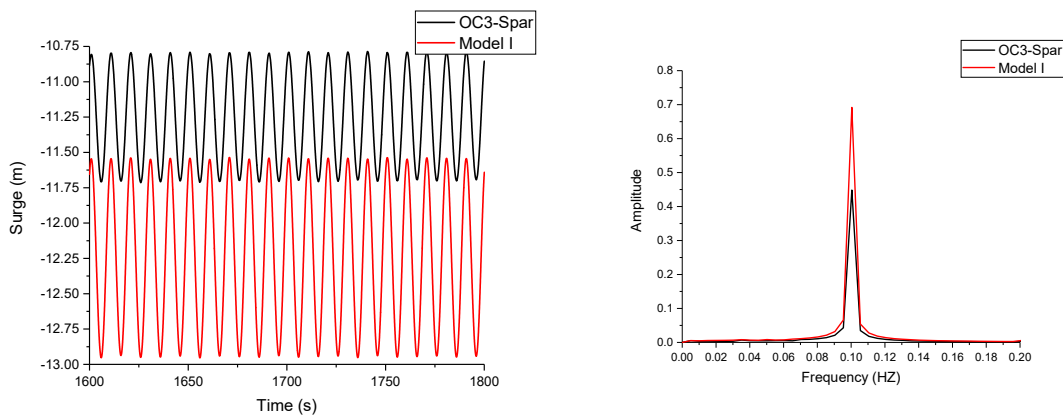
Figure 7: Surge motion phase plan for OC3-Hywind and Model-I.

6.1.2. Surge Response (LC 2)

Displacement time histories and Power spectrum densities for the two models of SFWT's are presented in figures 8 and 9, at 10 sec. wave period, 5m wave height and 10m/s wind velocity. The peak surge motion of the OC3-Hywind is about 11.25 m after reaching the stable state. However, the peak surge motion of the Model I is about 12.25 m after achieving the stable state. The surge motion of the OC3-Hywind model under the combination of wind and wave load case is smaller than that in the Model I as shown in Fig. 8-a, as the same under wave load case The wind has more sever effect on the transient response where drifted the spar for more than 11m for about 500 sec. then reached a stationary response where the oscillation is about a new equilibrium position. Indicating that the mean platform surge responses are mainly caused by the wind loads However, the standard deviation (fluctuation) of the platform surge is mainly caused by the wave loads as shown in the graph of The Power spectrum densities for the two models of SFWT's in Fig. 9-b, indicating that the response has a periodic pattern with maximum peak response at the wave excitation frequency (about 0.1 HZ) Statistics of the stationary motion are shown in Table 6.

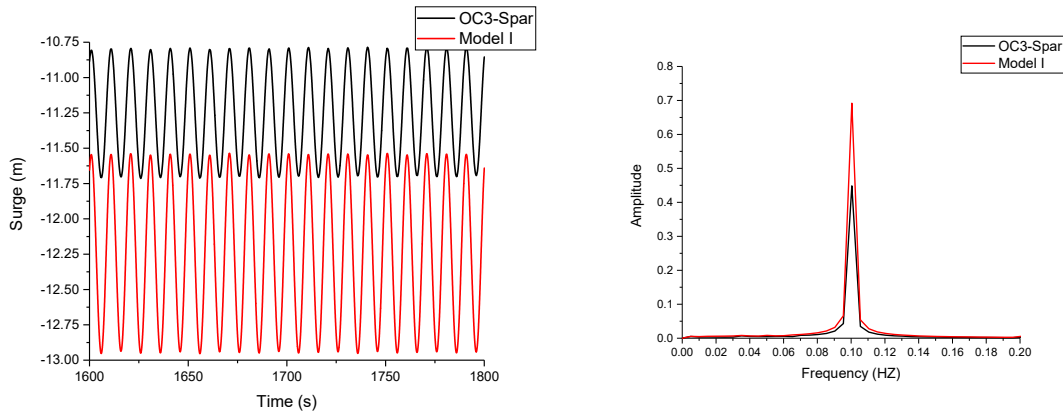


(p) Surge Motion from 0 to 1800 s (q) Surge Motion from 1600 s to 1800 s
Figure 8: Surge Response under LC 2, WHA= 0° and 90° for OC3-Hywind.



(a) Surge Motion from 1600 s to 1800 s (b) Power Spectrum Density
Figure 9: Surge Response under LC 2, WHA= 0° for OC3-Hywind and Model-I.

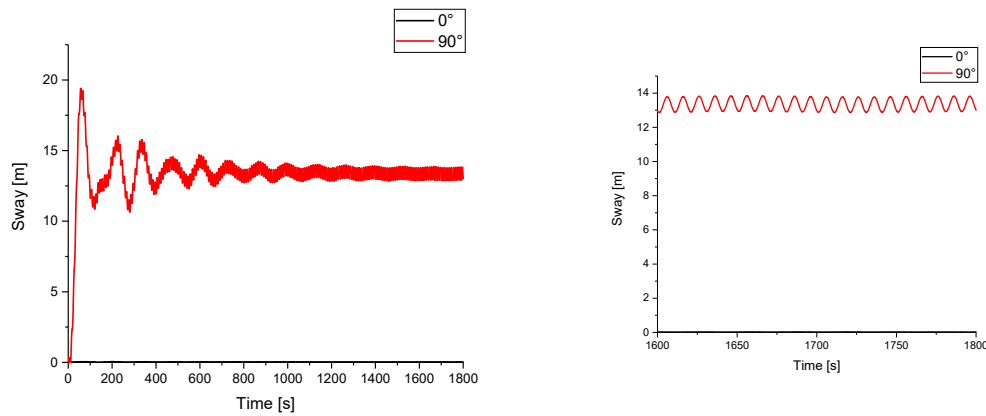
6.1.3. Sway Response (LC 1)



(c) Surge Motion from 1600 s to 1800 s (d) Power Spectrum Density
Figure 10: Sway response under LC 1, WHA= 0°, 30°, 60° and 90° for OC3-Hywind.

6.1.4. Sway Response (LC 2)

Displacement time histories for OC3-Hywind model are presented in fig. 11, at 10 sec. wave period, 5m wave height and 10m/s wind velocity. When the wave directions gradually change to 90 degrees, the sway motion response increases, see Fig. 11. The peak sway motion of the OC3-Hywind is about 13.35 m after reaching the stable state. The wind has more sever effect on the transient response where drifted the spar for more than 13m for about 500 sec. then reached a stationary response where the oscillation is about a new equilibrium position. Indicating that the mean platform surge responses are mainly caused by the wind loads However, the fluctuation of the platform surge is mainly caused by the wave loads.

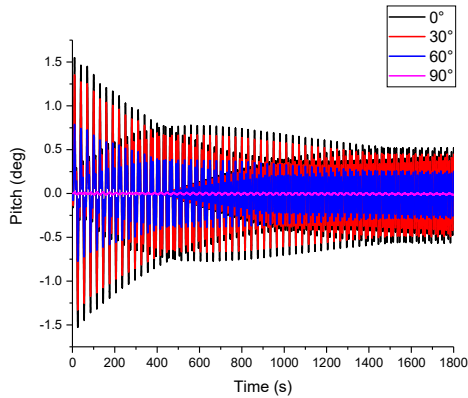


(e) Sway Motion from 0 to 1800 s (f) Sway Motion from 1600 s to 1800 s
Figure 11: Sway response under LC 1, WHA= 0°, 30°, 60° and 90° for OC3-Hywind

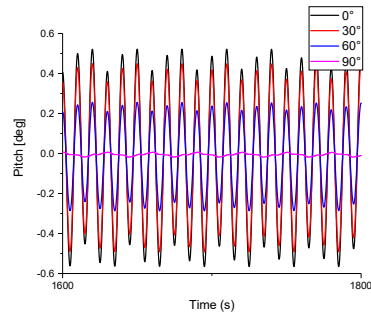
6.1.5. Pitch Response (LC 1)

Displacement time histories, Power spectrum densities and phase planes for the two models of SFWT’s are presented in figures 12, 13 and 14. The Pitch motion of the OC3-Hywind model is shown in Fig. 12 under different WHA (30, 60, and 90 degrees), It is obvious that waves of zero heading angles give the maximum response. The dynamic

response of pitching motion for the two models of SFWT's in Fig. 13-b exhibits two peaks, the natural frequency range of pitching (about 0.036 HZ) and the forcing wave frequency range (about 0.1 HZ). The phase planes of the two models of SFWT's shown in Fig. 14 shows that the steady state behavior is periodic and stable.

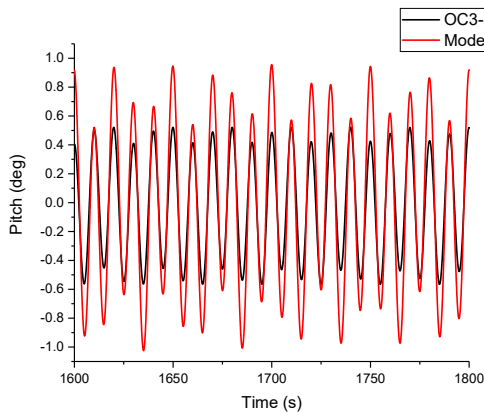


(g) Pitch Motion from 0 to 1800 s

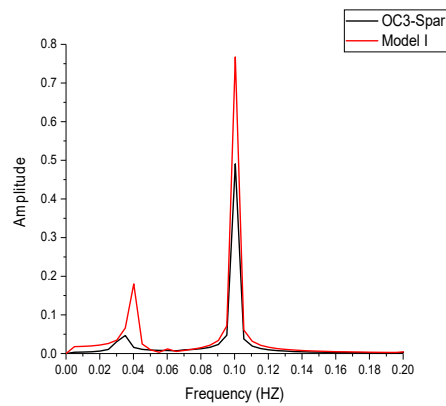


(h) Pitch Motion from 1600 s to 1800 s

Figure 12: Pitch Response under LC 1, WHA= 0°, 30°, 60° and 90° for OC3-Hywind.

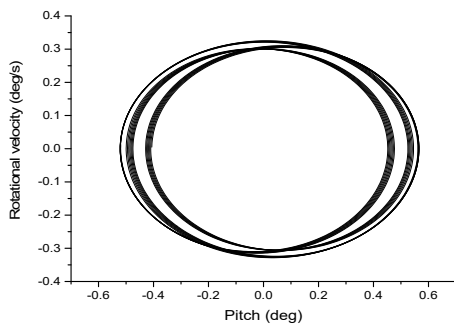


(i) Pitch Motion from 1600 s to 1800 s

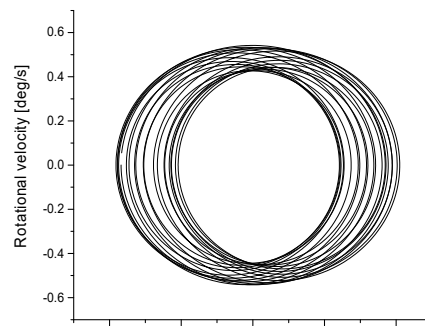


(j) Power Spectrum Density

Figure 13: Pitch Response under LC 1, WHA= 0° for OC3-Hywind and Model-I.



(k) Phase Plan for OC3-Hywind



(l) Phase Plan for Model-I

Figure 14: Pitch Motion Phase plan for OC3-Hywind and Model-I.

6.1.6. Pitch Response (LC 2)

Displacement time histories and Power spectrum densities for the two models of SFWT's are presented in figures 15 and 16, at 10s wave period, 5m wave height and 10m/s wind velocity. The mean pitch motion for the two models of SFWT's is about 3° under the effect of wind and wave loading which is less than the design pitch (about 5°). It should be mentioned that in the wind-wave case the first peak in Fig. 16 is much less than that of Fig. 13. This is due to the wind effect, which does not excite the modes near the natural frequencies of the pitch motion as in case of wave only load.

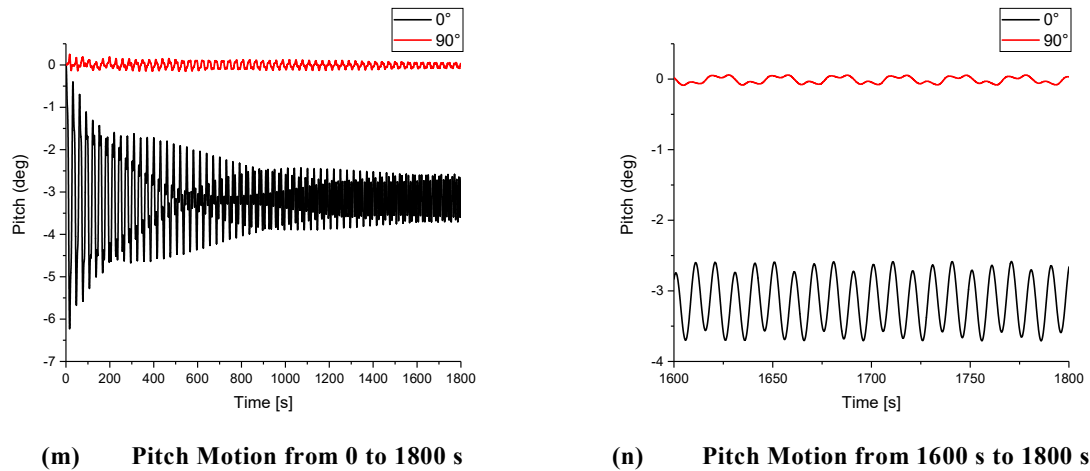


Figure 15: Pitch Motion Phase plan for OC3-Hywind and Model-I.

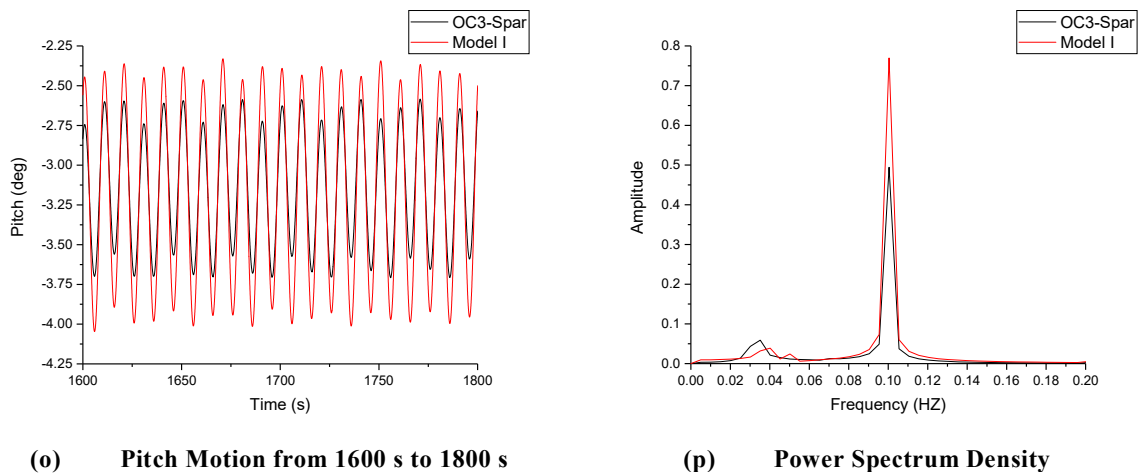
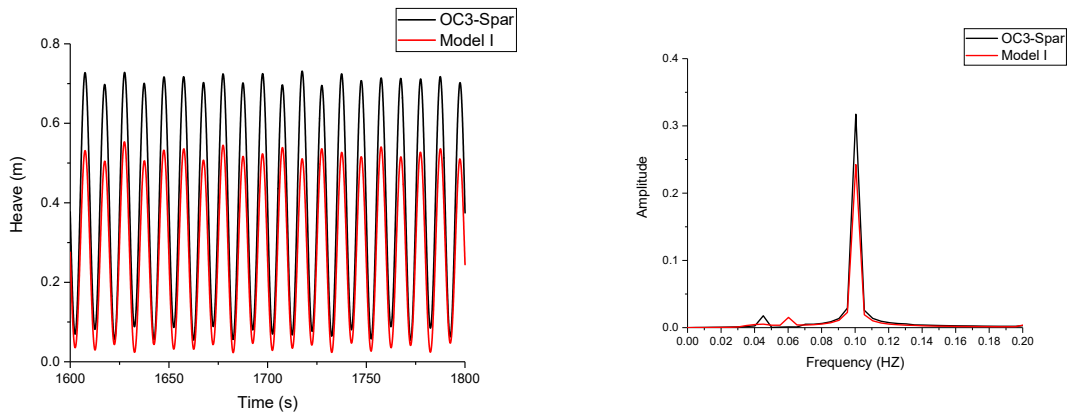


Figure 16: Pitch Response Under LC 2, WHA= 0° for OC3-Hywind and Model-I.

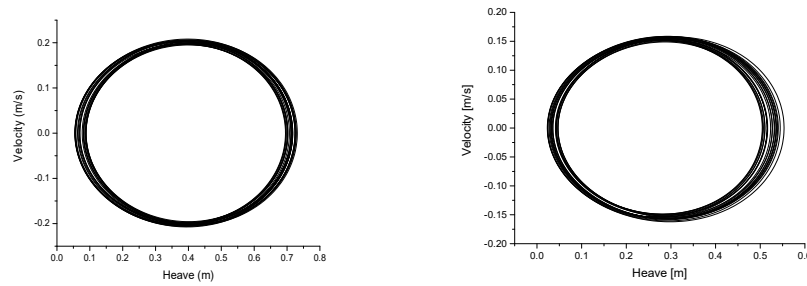
6.1.7. Heave Response

Displacement time histories, Power spectrum densities and phase planes for the two models of SFWT's are presented in figures 17, 18 and 19 in wave-only case and combined wind-wave case. The dynamic response for heave motion is not affected by angle change, indicating that the dynamic response of the wind turbine system produced by wave load is not affected by angle change. The displacement in heave significantly reduces with an increase in spar diameter during heave motion, when the spar diameter dominates over other design factors. Where the diameter of the Model I (13.09 m) is larger than the OC3-Hywind model (9.4 m) by 39.3% as shown in table 2 Similarly to the pitch motion,

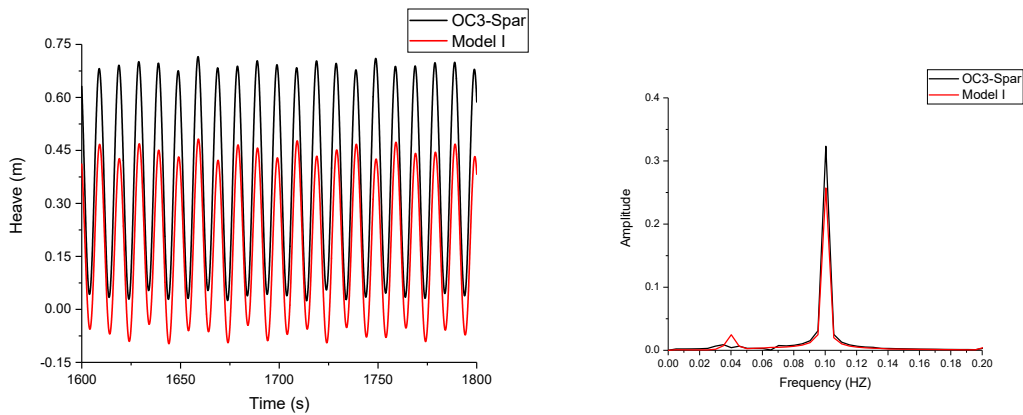
it can be found that the two responding peaks from the power spectra being the heave/pitch natural frequency zone and the wave frequency zone (about 0.1 HZ).



(q) Heave Motion from 1600 s to 1800 s (r) Power Spectrum Density
Figure 17: Heave Response under LC 1, WHA= 0° for OC3-Hywind and Model-I.



(s) Phase Plan OC3-Hywind (t) Phase Plan Model-I
Figure 18: Heave response under LC 1, WHA= 0° for OC3-Hywind and Model-I



(u) Heave Motion from 1600 s to 1800 s (v) Power Spectrum Density
Figure 19: Heave response under LC 2, WHA= 0° for OC3-Hywind and Model-I

Table: 5 Comparison of Natural Frequency

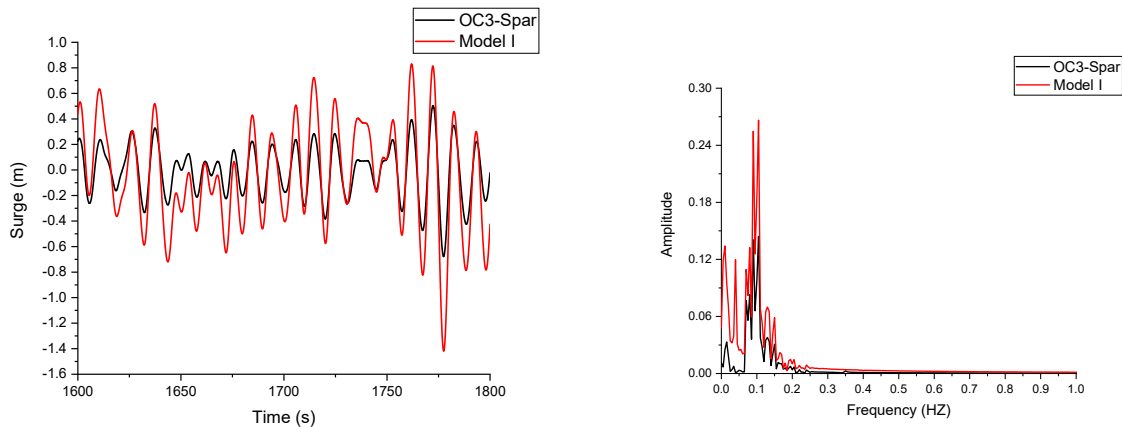
Load Case	DOF	OC3-Spar				Model I			
		Max.	Min.	Mean	SD	Max.	Min.	Mean	SD
LC2	Surge (m)	11.71	10.78	11.25	0.32	12.95	11.54	12.25	0.49
	Heave (m)	0.72	0.02	0.36	0.23	0.48	0.09	0.18	0.18
	Pitch (°)	3.71	2.58	3.15	0.36	4.04	2.33	3.18	0.55

6.2 IRREGULAR WAVE

Two SFWT models' motion response is examined under irregular wave conditions. It's hard to show the results using time domain signals because the motion reactions to irregular waves' time domain curves are random. Finally, FFT was used to produce the frequency domain motion spectra.

6.2.1 Surge Response (LC 3)

Displacement time histories, Power spectrum densities and phase planes for the two models of SFWT's are presented in figures 20 and 21. As shown in Fig. 20, about 0.01 Hz that's when the first peak of the platform's surge motion exhibits up This is close to the platform's natural frequency. The surge power spectral density has two peaks, one at the frequency of the structure and the other at the frequency of the wave. Despite the fact that the wave is irregular the phase plan in Fig. 21, shows a certain pattern for the motion. The notches in Fig. 20-a, indicates the contribution of the modes as indicated by the power spectrum in Fig. 20-b, i.e., the motion is not pure surge due to the nature of the wave which has multi frequency ranges that excite other modes.



(w) Surge Motion from 1600 s to 1800 s (x) Power Spectrum Density

Figure 20: Surge Response under LC 3, WHA= 0° for OC3-Hywind and Model-I.

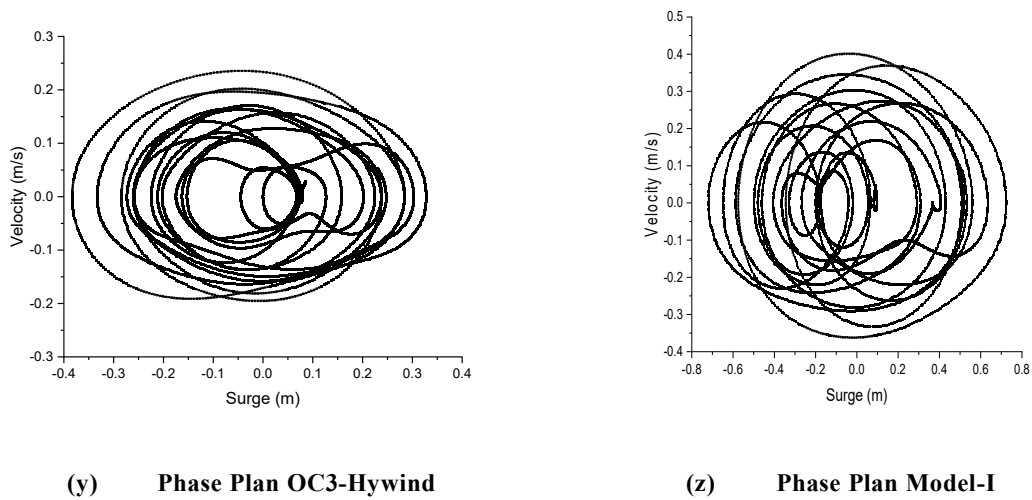


Figure 21: Surge Phase Plan for OC3-Hywind and Model-I.

6.2.2 Heave Response (LC 3)

Displacement time histories, Power spectrum densities and phase planes for the two models of SFWT's are presented in figures 22 and 23. It can be found that the two responding peaks from the power spectra being the heave/pitch natural frequency zone and the wave frequency zone (about 0.1 HZ). Despite the fact that the wave is irregular the phase plans in Fig. 23, shows a certain pattern for the motion. The notches in Fig. 22-a, indicates the contribution of the modes as indicated by the power spectrum in Fig. 22-b, i.e., the motion is not pure surge due to the nature of the wave which has multi frequency ranges that excite other modes.

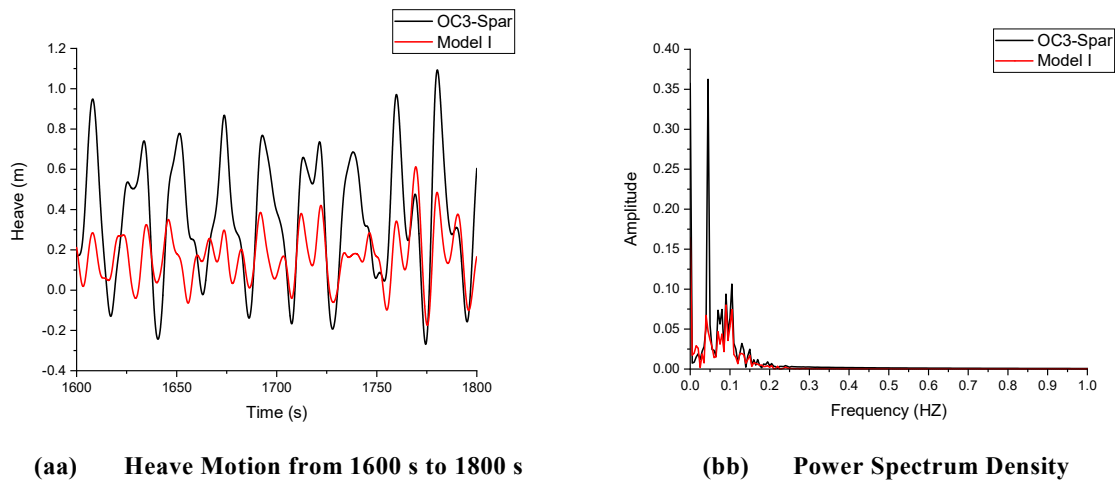
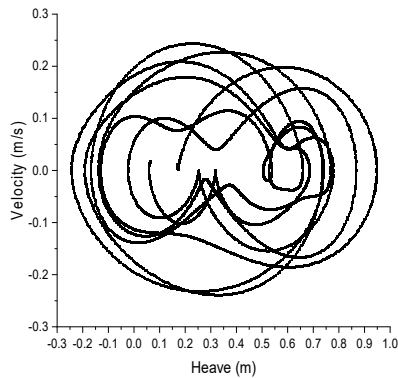
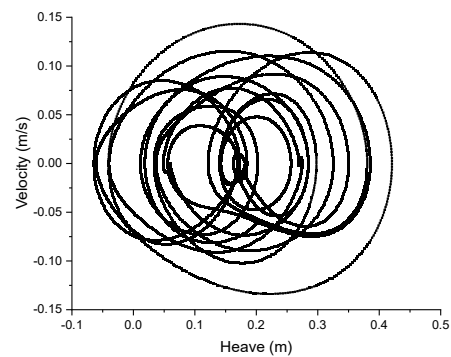


Figure 22: Heave Response under LC 3, WHA= 0° for for OC3-Hywind and Model-I.



(cc) Phase Plan OC3-Hywind

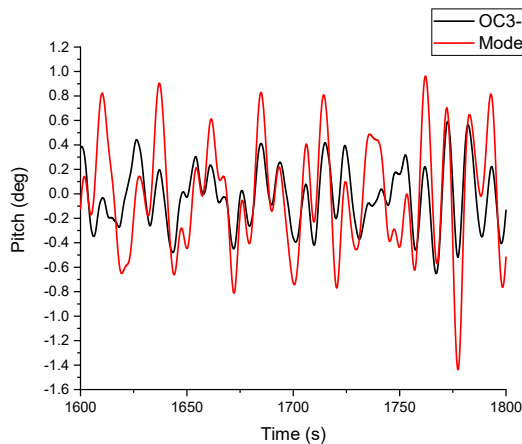


(dd) Phase Plan Model-I

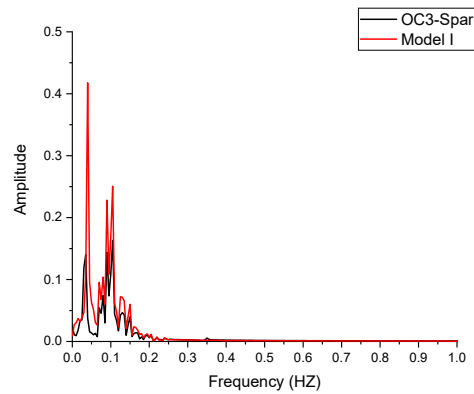
Figure 23: Heave Phase Plan for OC3-Hywind and Model-I.

6.2.3 Pitch Response (LC 3)

Displacement time histories, Power spectrum densities and phase planes for the two models of SFWT's are presented in figures 24 and 25. It can be found that the two responding peaks from the power spectra being the heave/pitch natural frequency zone and the wave frequency zone (about 0.1 HZ). Despite the fact that the wave is irregular the phase plan in Fig. 25, shows a certain pattern for the motion. The notches in Fig. 24-a, indicates the contribution of the modes as indicated by the power spectrum in Fig. 24-b, i.e., the motion is not pure surge due to the nature of the wave which has multi frequency ranges that excite other modes.



(ee) Pitch Motion from 1600 s to 1800 s



(ff) Power Spectrum Density

Figure 24: Heave Phase Plan for OC3-Hywind and Model-I.

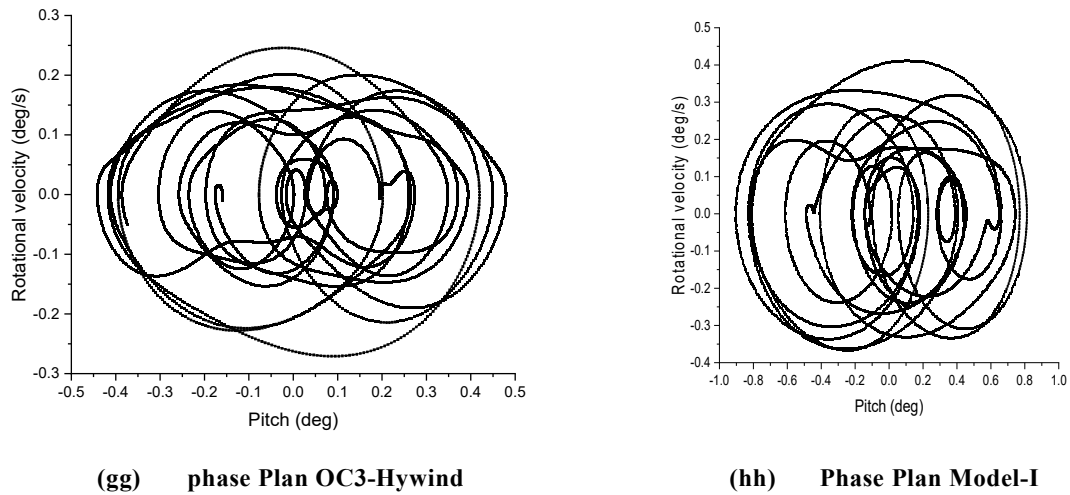


Figure 25: Pitch Phase Plan for OC3-Hywind and Model-I.

7. CONCLUSIONS AND RECOMMENDATIONS

In this investigation, a new model spar (Model I) compared with the (OC3-Hywind) spar type platform is presented. This investigation objective is to reduce response motions. The proposed model is expected to improve performance under various environmental conditions. This new model (Model I) can be more powerful so that heavier wind turbines, like a 10 MW wind turbine can be installed on it. This new model (Model I) is eligible for installation at a depth of 150 m.

- The height and diameter of the spar have an effect on the surge behavior. When the diameter and height of the spar get bigger, the structure will move less in the direction of the surge.
- Increasing spar diameter can reduce structural dynamic movements, which will improve the structure's overall stability. However, as the diameter of the spar increases, so does the structure's weight.
- The surge and pitch motions become less evident as the structure's height increases.
- The heave is significantly reduced by increasing the spar diameter of the structure.
- The spectrum responses for the two SFWT (OC3-Hywind and Model I) have a narrow-banded peaks at their natural frequencies and wave excitation in the power spectrum densities.

The results presented characterize the coupled dynamic response of a Spar-Type FOWT, helping to understand the dynamic characteristics of the Spar-Type FOWT, and thus help inform necessary changes to the initial design of the Spar-type FOWT. In the future, researches will look into the Spar-type FOWT in different depths and try a scaled model in a wave tank.

REFERENCES

1. *Abou-Rayan, A. M., & El-Gamal, A. R. (2013). Wave induced motion of a triangular tension leg platforms in deep waters. Ocean Systems Engineering, 3(2), 149-165. doi:10.12989/ose.2013.3.2.149*

2. Abou-Rayan, A. M., & Hussein, O. S. (2014). Dynamic Responses of Square TLP'S to Random Wave Forces. *International Journal of Civil Engineering (IJCE) Vol, 3*, 103-110.
3. Abou-Rayan, A. M., Khalil, N. N., & Afify, M. S. (2016). Dynamic behavior of TLP's supporting 5-MW wind turbines under multi-directional waves. *Ocean Systems Engineering*, 6(2), 203-216. doi:10.12989/ose.2016.6.2.203
4. Ansys, A. (2016). *AQWA user's manual release 17.0*. USA. Canonsburg (PA): ANSYS Inc.
5. Bashir, M. B. A. (2022). Principle Parameters and Environmental Impacts that Affect the Performance of Wind Turbine: An Overview. In *Arabian Journal for Science and Engineering (Vol. 47, pp. 7891-7909)*: Springer Science and Business Media Deutschland GmbH.
6. Crozier, A. (2011). *Design and dynamic modeling of the support structure for a 10MW offshore wind turbine*. Master's thesis.
7. Díaz, H., & Guedes Soares, C. (2020). Review of the current status, technology and future trends of offshore wind farms. In *Ocean Engineering (Vol. 209)*: Elsevier Ltd.
8. Duan, F., Hu, Z., & Niedzwecki, J. M. (2016). Model test investigation of a spar floating wind turbine. *Marine Structures*, 49. doi:10.1016/j.marstruc.2016.05.011
9. Hasselmann, K., Barnett, T. P., Bouws, E., Carlson, H., Cartwright, D. E., Enke, K., . . . Kruseman, P. (1973). Measurements of wind-wave growth and swell decay during the Joint North Sea Wave Project (JONSWAP). *Ergaenzungsheft zur Deutschen Hydrographischen Zeitschrift, Reihe A*.
10. Hussein, K. R., Hussein, A. W., Hegazy, E. H., & Amin, A. A. (2013). Structural design of a floating foundation for offshore wind turbines in red sea. Paper presented at the Analysis and Design of Marine Structures - Proceedings of the 4th International Conference on Marine Structures, MARSTRUCT 2013.
11. Jeon, S. H., Cho, Y. U., Seo, M. W., Cho, J. R., & Jeong, W. B. (2013). Dynamic response of floating substructure of spar-type offshore wind turbine with catenary mooring cables. *Ocean Engineering*, 72. doi:10.1016/j.oceaneng.2013.07.017
12. Jonkman, J. (2010). *Definition of the Floating System for Phase IV of OC3*. Retrieved from
13. Jonkman, J., Butterfield, S., Musial, W., & Scott, G. (2009). *Definition of a 5-MW reference wind turbine for offshore system development*. Retrieved from
14. Jonkman, J. M., & Buhl Jr, M. L. (2005). *FAST user's guide*. Golden, CO: National Renewable Energy Laboratory, 365, 366.
15. Jonkman, J. M., & Matha, D. (2011). Dynamics of offshore floating wind turbines-analysis of three concepts. *Wind Energy*, 14(4). doi:10.1002/we.442
16. Karimirad, M., & Moan, T. (2012). Wave- and Wind-Induced Dynamic Response of a Spar-Type Offshore Wind Turbine. *Journal of Waterway, Port, Coastal, and Ocean Engineering*, 138(1). doi:10.1061/(asce)ww.1943-5460.0000087

17. Matsukuma, H., & Utsunomiya, T. (2008). Motion analysis of a floating offshore wind turbine considering rotor-rotation. *IES Journal Part A: Civil and Structural Engineering*, 1(4), 268-279. doi:10.1080/19373260802401702
18. Myhr, A., Maus, K. J., & Nygaard, T. A. (2011). Experimental and computational comparisons of the OC3-HYWIND and Tension-Leg-Buoy (TLB) floating wind turbine conceptual designs. Paper presented at the Proceedings of the International Offshore and Polar Engineering Conference.
19. Oyejobi, D. O., Jameel, M., & Sulong, N. H. R. (2017). Stochastic Response of Intact and a Removed Tendon Tension Leg Platform to Random Wave and Current Forces. *Arabian Journal for Science and Engineering*, 42(3). doi:10.1007/s13369-016-2282-4
20. Qu, X., Li, Y., Tang, Y., Hu, Z., Zhang, P., & Yin, T. (2020). Dynamic response of spar-type floating offshore wind turbine in freak wave considering the wave-current interaction effect. *Applied Ocean Research*, 100. doi:10.1016/j.apor.2020.102178
21. Sethuraman, L., & Venugopal, V. (2013). Hydrodynamic response of a stepped-spar floating wind turbine: Numerical modelling and tank testing. *Renewable Energy*, 52. doi:10.1016/j.renene.2012.09.063
22. Shin, H. (2011). Model test of the OC3-Hywind floating offshore wind turbine. Paper presented at the Proceedings of the International Offshore and Polar Engineering Conference.
23. Soares-Ramos, E. P. P., de Oliveira-Assis, L., Sarrias-Mena, R., & Fernández-Ramírez, L. M. (2020). Current status and future trends of offshore wind power in Europe. *Energy*, 202. doi:10.1016/j.energy.2020.117787
24. Tafazzoli, S., Shafaghat, R., & Alamian, R. (2021). Optimization study of a catenary mooring system for a spar floating wind turbine based on its hydrodynamic responses. *Proceedings of the Institution of Mechanical Engineers Part M: Journal of Engineering for the Maritime Environment*, 235(2), 657-674. doi:10.1177/1475090220917812
25. Wen, B., Jiang, Z., Li, Z., Peng, Z., Dong, X., & Tian, X. (2022). On the aerodynamic loading effect of a model Spar-type floating wind turbine: An experimental study. *Renewable Energy*, 184, 306-319. doi:10.1016/j.renene.2021.11.009
26. Yu, M., Hu, Z.-q., & Xiao, L.-f. (2015). Wind-wave induced dynamic response analysis for motions and mooring loads of a spar-type offshore floating wind turbine. *Journal of Hydrodynamics, Ser. B*, 26(6), 865-874.
27. Yue, M., Liu, Q., Li, C., Ding, Q., Cheng, S., & Zhu, H. (2020). Effects of heave plate on dynamic response of floating wind turbine Spar platform under the coupling effect of wind and wave. *Ocean Engineering*, 201. doi:10.1016/j.oceaneng.2020.107103
28. Zheng, Z., Chen, J., Liang, H., Zhao, Y., & Shao, Y. (2020). Hydrodynamic responses of a 6 MW spar-type floating offshore wind turbine in regular waves and uniform current. *Fluids*, 5(4). doi:10.3390/fluids5040187